ELECTRONIC SUPPLEMENTARY INFORMATION

Sensitivity optimization in pulse EPR experiments with photo-labels by multiple-echo-integrated dynamical decoupling

Natalya E. Sannikova,[a,b] Anatoly Melnikov,[a,b] Sergey L. Veber,[a,b] Olesya A. Krumkacheva,[a,b*] Matvey V. Fedin [a,b*]

[a] International Tomography Center SB RAS, 630090 Novosibirsk, Russia

[b] Novosibirsk State University, Pirogova Str. 2, Novosibirsk 630090, Russia

* Email addresses: olesya@tomo.nsc.ru (O.A.K), mfedin@tomo.nsc.ru (M.V.F.)

Table of contents

1. Implementation of the external digitizer instead of the default SpecJetII

The characteristics of the M4i.2211 digitizer are excellent for routine EPR measurements and include proper vertical and horizontal resolutions that are 8 bit and 1.25 GS/s, respectively, fast 80 samples re-arm time, a possibility to use an external clock frequency, and high-speed data transmission up to 3.5 GB/s, which were achieved via PCIe-x8 of the second generation. A simple calculation shows that even 100 MB of data will be transferred to a PC in a decent 30 ms. Taking into account the 8-bit resolution, 100 MB of data contain a signal approximately 85 ms long at the maximum sample rate of the digitizer. This is more than enough for the proposed CPMG detection scheme. In the performed experiments, the pulse sequence and other settings of the spectrometer were set in the Bruker Xepr software, while the external digitizer was controlled using the open source software Atomize (https://github.com/Anatoly1010/Atomize)[1] on a separate PC. The actual recording, averaging, and drawing of experimental two-dimensional data was also accomplished in Atomize using a simple experimental script in which the number of shots was synchronized with the Bruker software. In Atomize, graphs are plotted by the highly productive graphics library pyqtgraph 0.13.1 (https://www.pyqtgraph.org/) using a server-client approach. Our experience shows that using 10 shots per point, a repetition rate up to 70 Hz can be achieved without missing any acquisition trigger when drawing in real time the entire experimental data set of approximately 300 by 35000 points. Higher repetition rates up to 200–500 Hz can be used with more shots per point, giving more time to complete the drawing. Alternatively, one can plot only the most important part of the data, which greatly reduces the size of the array. The size of the array is a limiting factor because the 8-bit output signal from the digitizer is inevitably converted to 32-bit or even 64-bit floating-point numbers to correctly average the data.

2. Optimal CPMG delays

The practical limit of delay τ in CPMG scheme is set by a spectrometer deadtime between ESE and the microwave (mw) pulse, which is set by a protection (defense) pulse. The defense pulse prohibits ESE detection both prior and after the mw pulse, with the corresponding configuration-set time delays. In some cases, ESE can be undetectable fully or partly because the next mw pulse is too close. Deadtimes between the mw π pulses cannot be totally eliminated and might differ for different spectrometer configurations and mw bands. In our study, the optimal and minimum CPMG pulse separation time τ was determined, at which the maximum SNR gain is achieved.

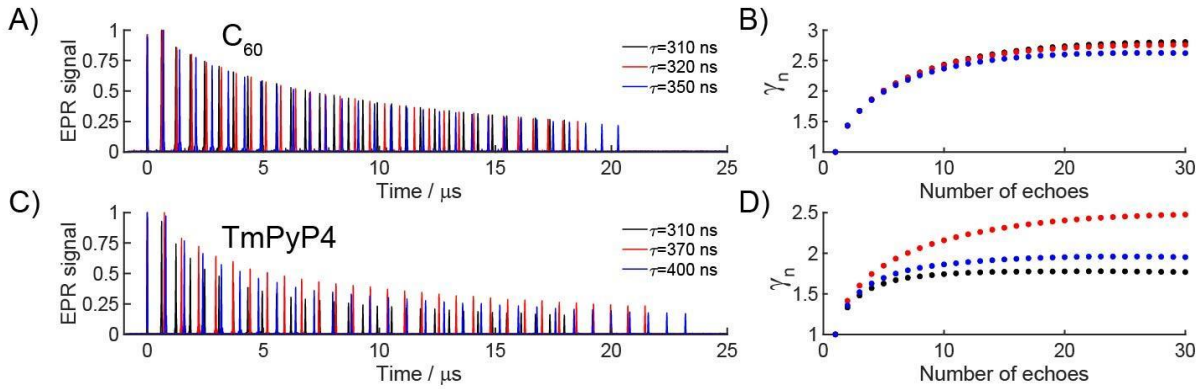

Figure S1. (A, C) The transient traces (in absolute values) detected upon photoexcitation of C_{60} in C_{60}TAM (A) and TmPyP4 (C), obtained using CPMG sequence with 30 echoes and different delays τ between mw pulses (Q-band). Right panels (B, D) show the corresponding SNR gains as a function of the number of integrated echoes. The same color codes are used in (A,B) and (C,D), respectively. All data are normalized to the corresponding SNR at n=1.

Figure S1 demonstrates time traces of the CPMG echo decays for C_{60} in C_{60}TAM/toluene and TmPyP4 in deuterated solvent at Q-band. The shortest Q-band delay (310 ns) was found to be the optimal delay for C_{60} providing the highest SNR gain. The presence of strong ESEEM modulation for TmPyP4, which results from porphyrin core nitrogens, makes optimal τ value at Q-band to be 370 ns; i.e., in this case the shortest delay is not the optimal one.

Compared to photo-excited molecules, TAM echoes are broader (FWHM of echoes: 62 ns for TAM, 30 ns for C_{60}, and 26 ns for TmPyP4), which also has an impact on the value of τ. Because the shape of the echo becomes cut at the edge at τ ≤340 ns (Figure S2), the minimum τ value was set to 350 ns.

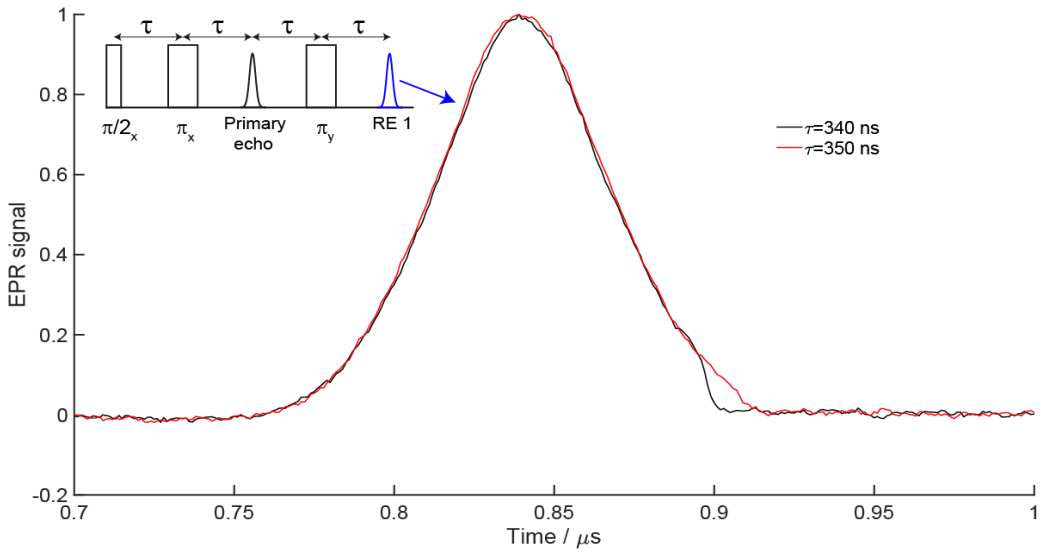

Figure S2. Q-band TAM echoes with two different τ delays between π mw pulses (indicated). Inset: pulse sequence with highlighted (blue line) first refocused echo (RE 1).

3. Optimization of the integration window width

Figure S3 shows SNR dependence on the width of the integration window for all pulse experiments. In case of ReLaserIMD, the obtained distance distributions and modulation depth values decreased as the echo integration gate increased; therefore, the width of the integration window was set to 40 ns to obtain sufficient modulation depth and SNR.

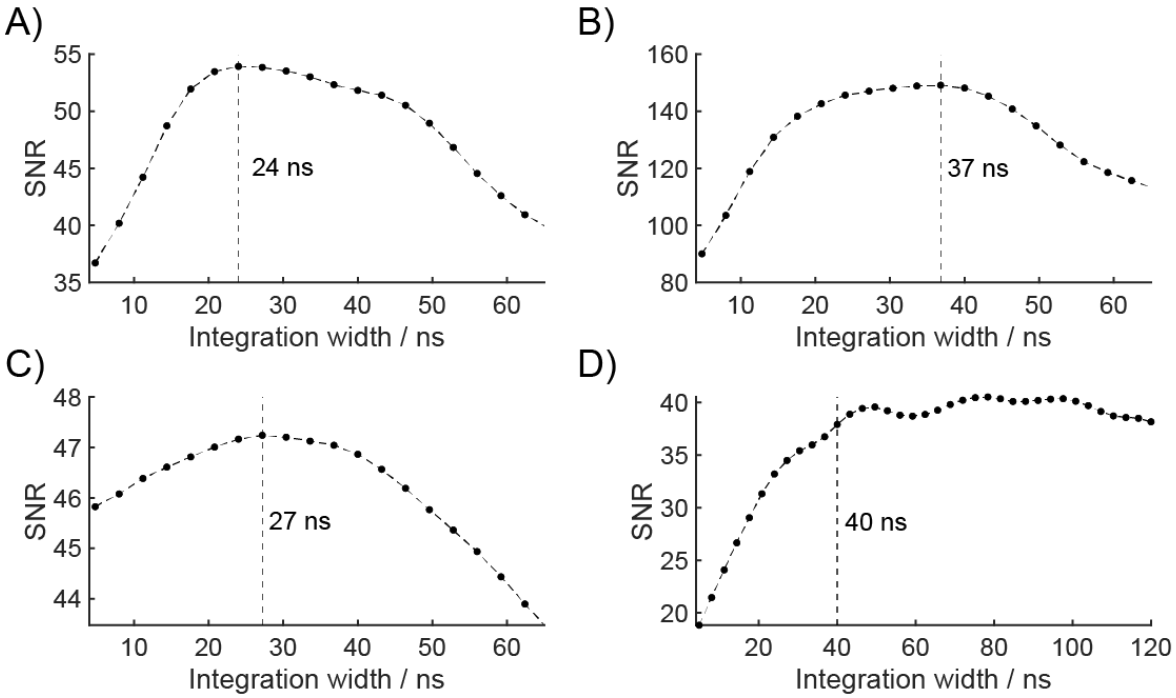

Figure S3. SNR as a function of the width of the integration window. Results for ED EPR experiments: (A) TmPyP4, (B) C_{60} in C_{60}TAM. Results for the pulse dipolar experiments: (C) detection of C_{60} in LiDEER, (D) detection of TAM in ReLaserIMD.

4. EPR data processing

- The noise level in echo-detected EPR spectra was measured as a standard deviation (SD) for the off-resonance signal.
- The following processing procedure was used for the DEER and ReLaserIMD experiments:

1. The original time domain traces $S_n(t)$ after integration of n echoes were background corrected using an exponential background:

$$I_n(t) = \frac{S_n(t)}{exp(-\alpha t)}.$$

2. The absolute value of modulation depth λ_n was defined as the difference between dipolar signal at zero time $I_n(0)$ and a constant value at which the signal plateaus (Fig. S4).
3. In order to define noise level, original dipolar time traces (before baseline subtraction) were smoothed from 100 ns using a 20-points gaussian-weighted moving average filter. The standard deviation (SD) of the dipolar traces was calculated after the smoothed curve was subtracted. SNR(n) was obtained as the ratio of λ_n (signal) and SD(noise):

$$Experimental\ SNR\ gain\ (n) = \frac{\lambda_n}{SD(noise)}.$$

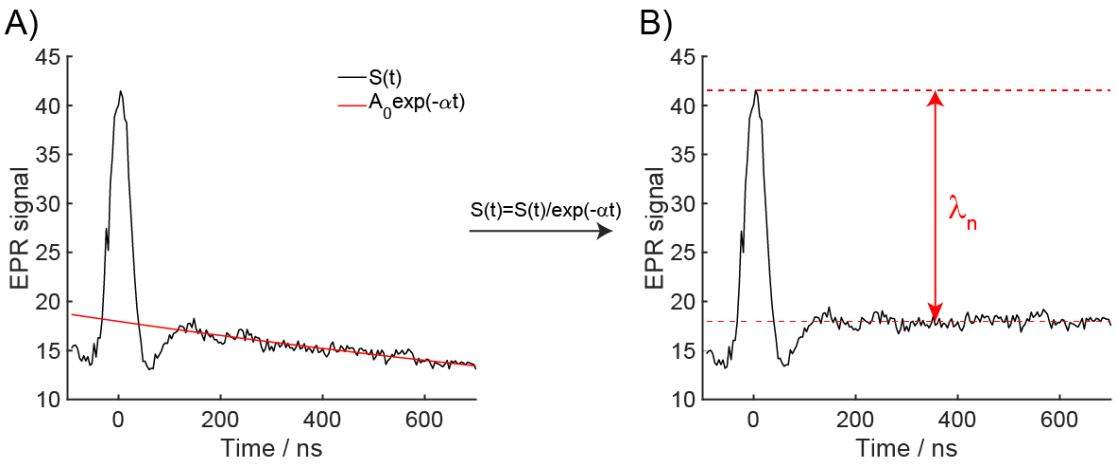

Figure S4. Data processing, illustrated using X-band LiDEER time-domain data for C_{60}TAM/toluene after integration of 29 echoes in CPMG block. (A) Primary time trace S(t) (black) and exponential background fitting (red). (B) The background-corrected data. The value of λ_n is shown by red arrow.

5. SNR gain for TAM under light irradiation

Figure S5 demonstrates that echoes in CPMG train for TAM in C_{60}TAM decay faster vs. time under irradiation with light. We first hypothesized that this extra drop occurred because of local heating induced by laser irradiation. To verify this, we measured the electron spin-lattice relaxation time T_1 under the light and in the dark, because it is temperature-dependent. We found that T_1 decreases from 18 μs to 16 μs under laser irradiation at 30 K. Even stronger change in T_1 occurs when the sample temperature is increased by about 6 K (Fig. S5), meaning that actual heating effect is below 6 K, supposedly around 3-4 K.

The right panel of Fig. S5 compares echoes vs. time in CPMG sequence for TAM at 30 K and 36 K. The nearly identical CPMG traces at 30 K and 36 K show that the laser-induced sample heating cannot be responsible for the observed shortening of T_{CMPG} under illumination. Therefore, most likely, the observed effect owes to the light-induced appearance of partner (C_{60}) spin and dipole-dipole interaction TAM-C_{60} within spin dyad.

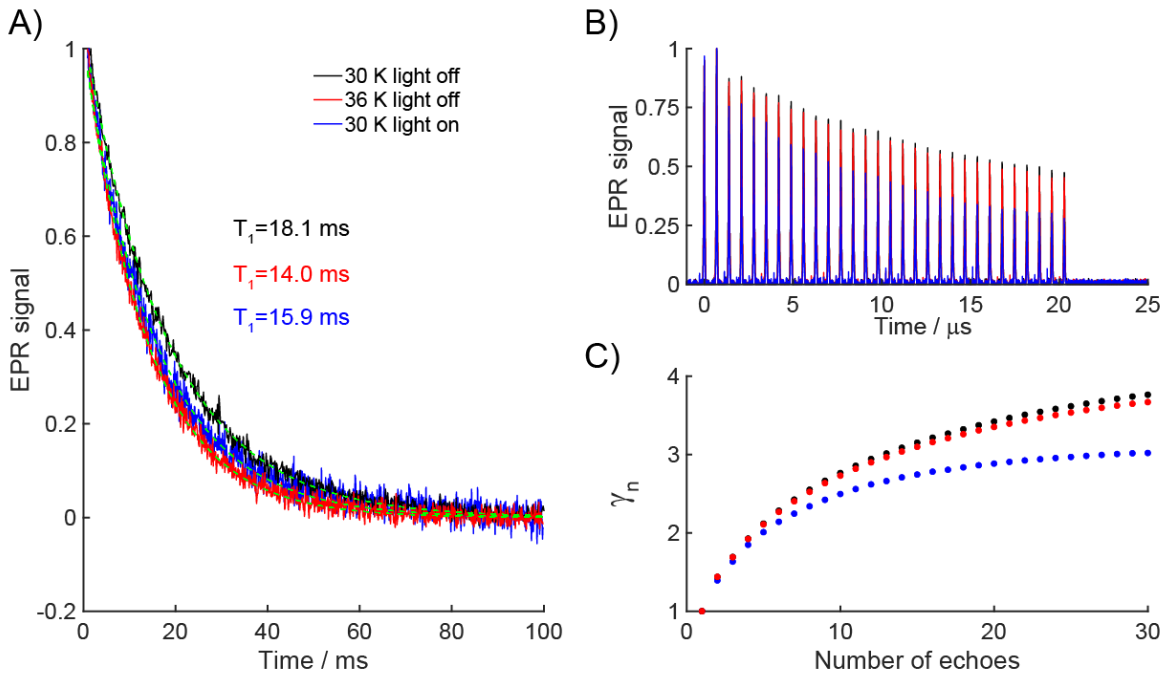

Figure S5. (A) Inversion recovery measurements for TAM in C_{60}TAM/toluene in the dark at 30 K (black), 36 K (red), and under light at 30 K (blue). Exponential function fits are shown by green. Inserted numbers correspond to T_1 values obtained from the fitting. (B) The normalized transient traces (in absolute values) detected using CPMG sequence with 30 echoes. (C) The corresponding SNR gains as functions of the number of integrated echoes. All data are normalized to the corresponding SNR at n=1. Color codes are the same in (A, B, C).

6. SNR gain for TAM in the dark

Figure S6 displays normalized time traces obtained upon application of CPMG without light irradiation for TAM in C60TAM and corresponding experimental and extrapolated SNR gains.

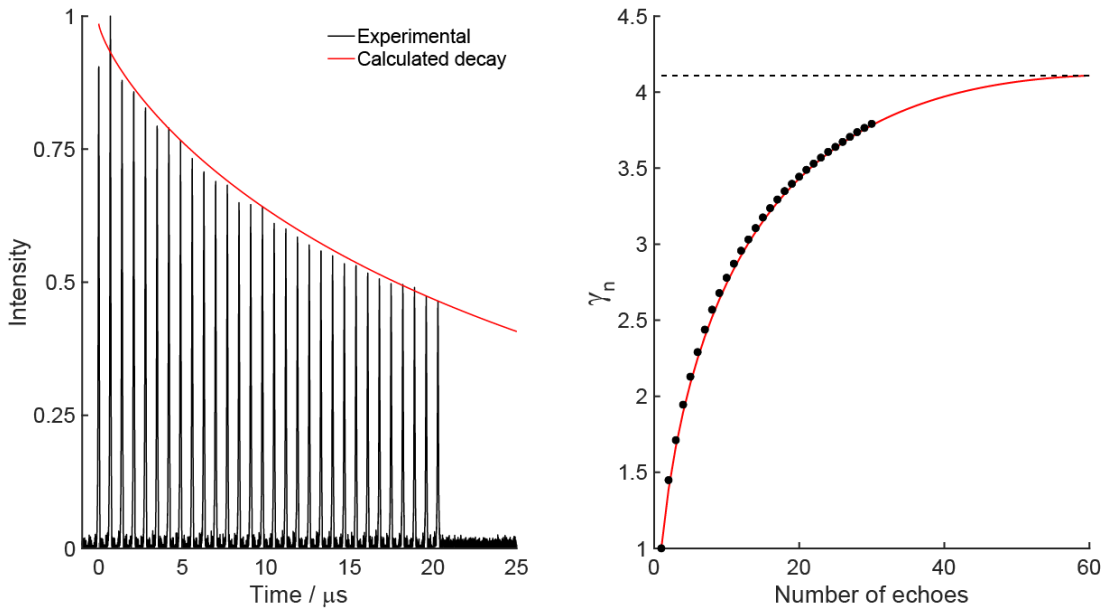

Figure S6. (A) Normalized transient traces (in absolute values) detected for TAM in C_{60}TAM using CPMG sequence with 30 echoes; in the dark (Q-band). The red line shows best fit obtained using a stretched exponential function (Eq. (1)) with T_{CMPG}=29.4 µs and p=0.8. (B) Corresponding experimental (black symbols) and extrapolated (red line) SNR gains as a function of the number of integrated echoes. All data are normalized to the corresponding SNR at n=1.

7. Distance distributions in LiDEER and ReLaserIMD with CMPG detection

The analysis of the DEER data was carried out in DeerAnalysis2019[2] using DEERNet approach[3]. The distance distribution was found to be nearly the same for any number of integrated echoes (Fig. S7).

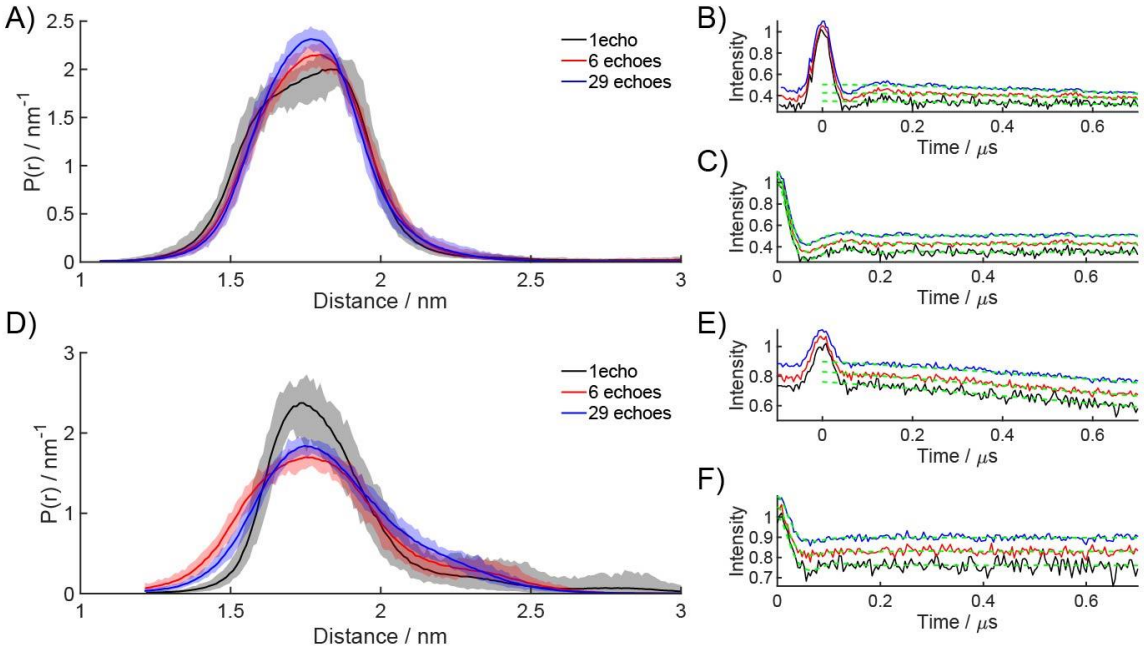

Figure S7. X-band LiDEER (A, B, C) and Q-band ReLaserIMD (D, E, F) data obtained using different numbers of integrated echoes in CMPG: (A, D) Distance distributions normalized to the modulation depth with uncertainty margins; (B, E) Raw time traces and their background fitting (green dashed line) (C, F) Traces after background correction and their fits using DEERNet approach (green dashed line). All time traces are shifted vertically for clarity.

8. LiDEER and ReLaserIMD modulation depth changes

Figure S8 demonstrates the dependence of the modulation depth in the number on integrated echoes for LiPDS experiments.

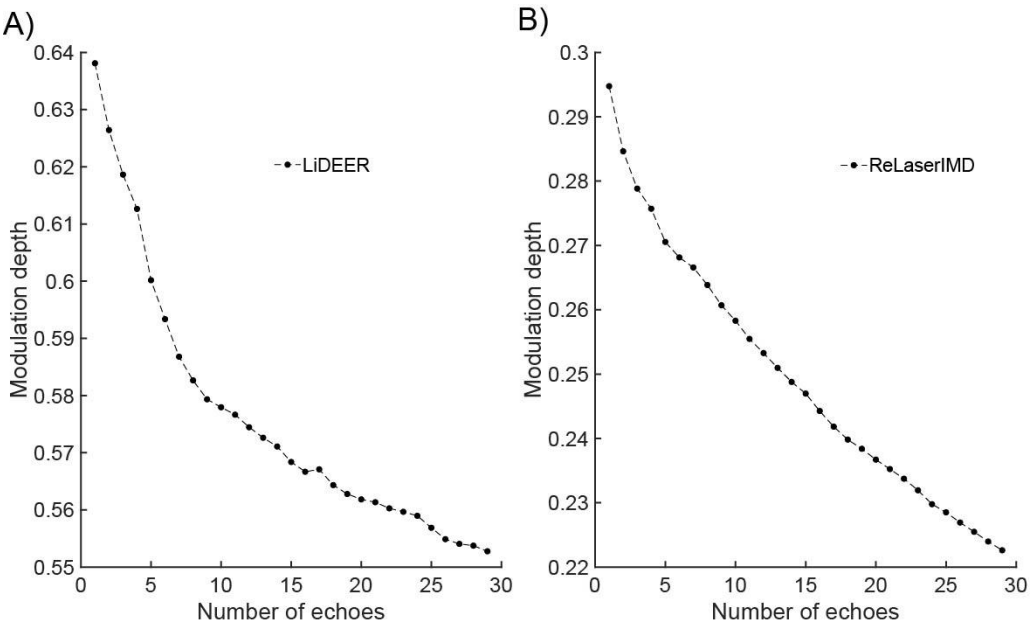

Figure S8. The dependence of the modulation depth (normalized to echo intensity) on the number of integrated echoes for X-band LiDEER (A) and Q-band ReLaserIMD (B) for 120 μM C_{60}TAM/toluene.

9. Laser pulse profile

Figure S9 demonstrates the laser pulse profile and width of the integration window.

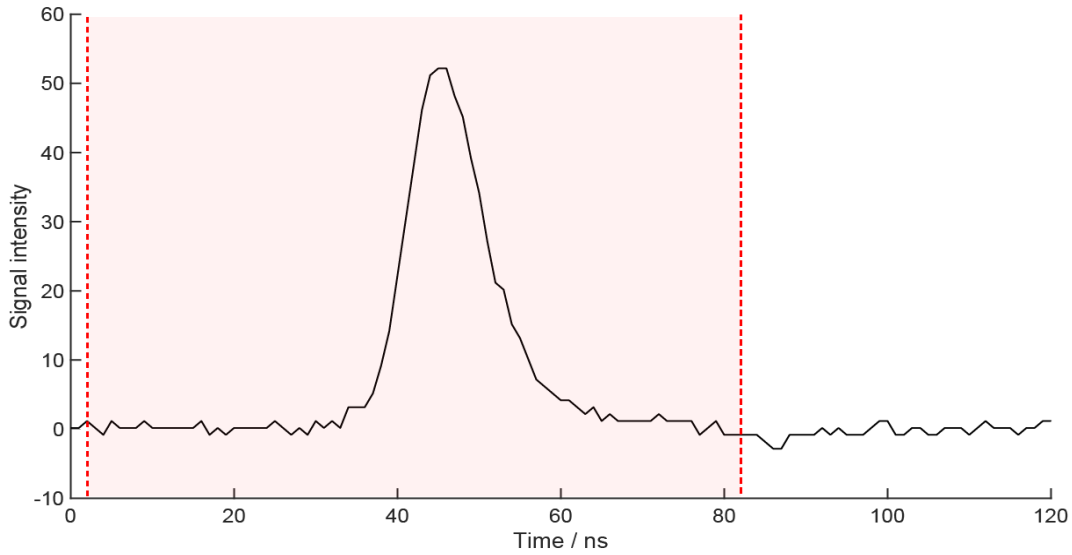

Figure S9. Laser pulse profile obtained using a fast photodiode (Thorlabs DET10C/M). Highlighted area shows the width of the integration window.

10. Noise analysis in LiPDS

SNR for the CPMG detection scheme with n echoes is defined as:

$$SNR(n) = \frac{\lambda_n}{\sigma_n} = \frac{\lambda_n}{\sqrt{\sigma_{laser,n}^2 + \sigma_{spec,n}^2}} = \frac{\lambda_n}{\sqrt{(\varepsilon_{laser,n}\boldsymbol{I_n})^2 + (\varepsilon_{spec,n}\boldsymbol{I_n})^2}},$$

Integration of multiple echoes in CPMG reduces $\varepsilon_{spec,n}$ as long as γ_n>1:

$$\varepsilon_{spec,n} = \frac{\sigma_{spec,n}}{I_n} = \frac{\sqrt{n}\,\sigma_{spec,1}}{I_n} = \frac{\varepsilon_{spec,1}}{\gamma_n},$$

whereas the addition of CPMG refocused echoes has no effect on $\varepsilon_{laser} = \varepsilon_{laser,1} = \varepsilon_{laser,n}$.

Taking this into account, SNR is described as:

$$SNR(n) = \frac{\lambda_n}{\sqrt{(\varepsilon_{laser}\boldsymbol{I_n})^2 + (\frac{\varepsilon_{spec,1}}{\gamma_n}\boldsymbol{I_n})^2}},$$

The SNR gain is then obtained as follows:

$$\frac{SNR(n)}{SNR(1)} = \frac{\lambda_n}{\sqrt{(\varepsilon_{laser}\boldsymbol{I_n})^2 + (\frac{\varepsilon_{spec,1}}{\gamma_n}\boldsymbol{I_n})^2}} \cdot \frac{\sqrt{(\varepsilon_{laser}\boldsymbol{I_1})^2 + (\varepsilon_{spec,1}\boldsymbol{I_1})^2}}{\lambda_1} = \frac{\lambda_n \boldsymbol{I_1}\sqrt{(\varepsilon_{laser})^2 + (\varepsilon_{spec,1})^2}}{\lambda_1 \boldsymbol{I_n}\sqrt{(\varepsilon_{laser})^2 + (\frac{\varepsilon_{spec,1}}{\gamma_n})^2}},$$

Using Eq.(1) and Eq. (2) from the main text, the final SNR gain is:

$$\frac{SNR(n)}{SNR(1)} = \frac{\beta_n}{\gamma_n}\frac{\sqrt{(\varepsilon_{laser})^2 + (\varepsilon_{spec,1})^2}}{\sqrt{(\varepsilon_{laser})^2 + (\frac{\varepsilon_{spec,1}}{\gamma_n})^2}},$$

The dipolar data were obtained by integration of echoes over a selected time range. Thus, it is necessary to regard the noise level resulting after a similar integration when discussing σ_{spec}. Therefore, to calculate σ_{spec} we have integrated 50 different time ranges in transient traces located after all echoes (noise area without signal) with the same width of the integration window as for the observed echoes. As a result, a set of 50 values of the integrals was obtained. The standard deviation of the resulting data was then calculated to obtain σ_{spec}.

The value of laser power fluctuation was obtained by calculating of the standard deviation (SD) of laser pulse energy vs. time. The relative ε_{laser} was evaluated as a ratio of SD to mean value of the laser pulse energy.

Figure S10 shows experimental $\left(\frac{\varepsilon_{spec,1}}{\gamma_n}\right)$ and (ε_{laser}) as a function of the number of integrated echoes with different concentrations of C_{60}TAM/toluene for all LiPDS experiments. ε_{laser} becomes comparable with $\varepsilon_{spec}/\gamma_n$ at n>20 for 120 μM of C_{60}TAM in LiDEER, yielding noticeable decrease in the maximum experimental SNR gain value (Fig.S10(A), Fig.5(C)). At the same time, ε_{laser} is negligible relative to $\varepsilon_{spec}/\gamma_n$ for any n in experiment with reduced concentration (Fig.S10(C)). The similar ratio between $\varepsilon_{spec}/\gamma_n$ and ε_{laser} were obtained in ReLaserIMD with low concentration

(Fig.S10(D)). The most dramatic effect of laser-induced noise on SNR gain occurred in ReLaserIMD with high concentration: $\varepsilon_{spec}/\gamma_n$ becomes less than ε_{laser} already at n=2, leading to a negligible experimental SNR gain (Fig.S10(B), Fig.5(D)).

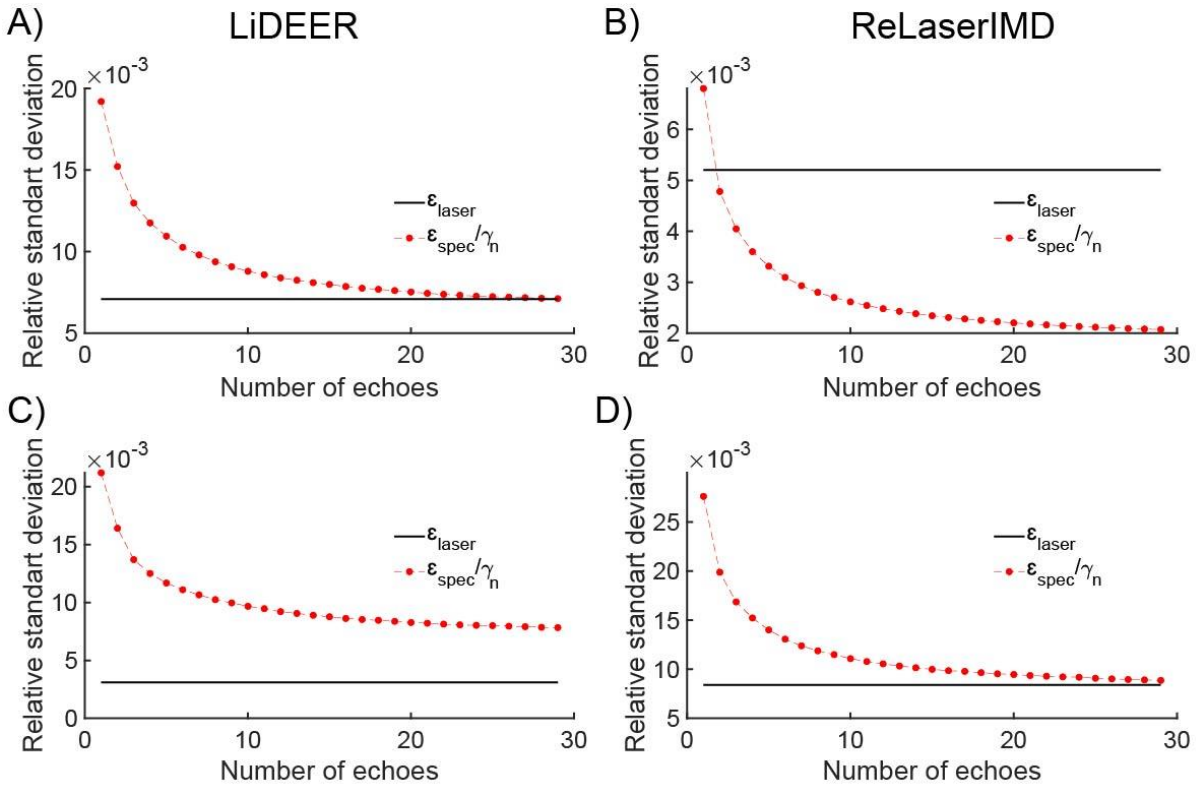

Figure S10. The value of $\left(\frac{\varepsilon_{spec,1}}{\gamma_n}\right)$ as a function of the number of integrated echoes for X-band LiDEER (A, C) and Q-band ReLaserIMD (B, D). The concentrations of C_{60}TAM/toluene are 120 μM (A, B) and 24 μM (C, D). The constant relative standard deviation of laser noise (ε_{laser}) is shown as a solid black line.

11. Fluctuation of laser pulse power vs. laser operation time

The relative standard deviation ε_{laser} depends on the laser operation time prior to experiment (Fig. S11). For our laser system, the decrease of the laser-induced noise level in LiPDS experiments can be achieved by a prolonged (3 or more days) laser operation prior to experiment.

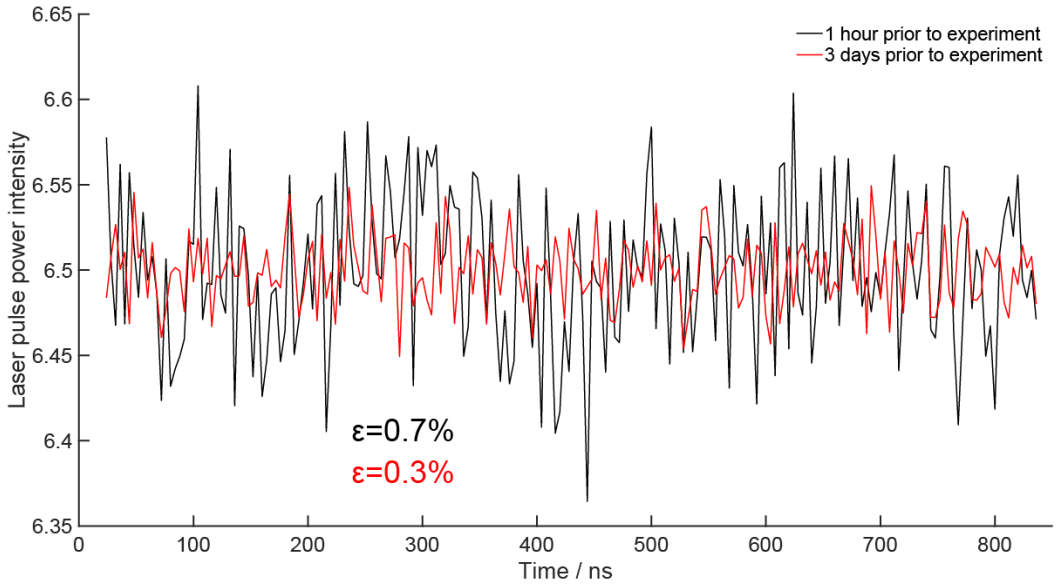

Figure S11. Laser pulse intensity time traces after 1 hour (black line) and 3 days (red line) laser operation prior to experiment. Inserted numbers show relative standard deviation.

12. SNR gain in ReLaserIMD experiments with reduced concentration (24 μM)

Figure S12 demonstrates SNR gains in ReLaserIMD experiments with $CPMG_n$ on C_{60}TAM/toluene obtained with reduced concentration (24 μM). The predicted "ab initio" SNR gain was calculated assuming $\sigma_{laser} = \varepsilon_{laser} \times \lambda_n$.

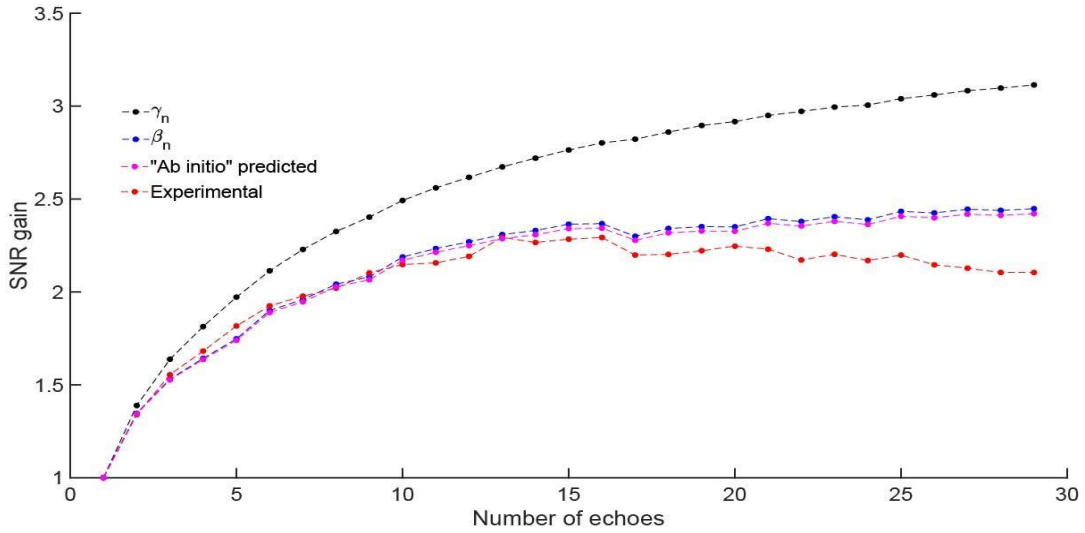

Figure S12. SNR gains vs. n in Q-band ReLaserIMD experiments with $CPMG_n$ blocks (n=1-29) on C_{60}TAM/toluene with reduced concentration (24 μM). The expected values γ_n obtained using eq.(2) (black line), the values β_n corrected relative to the modulation depth, given by eq.(3) (blue line), experimental SNR gain (red line), and SNR gain predicted "ab initio" assuming $\sigma_{laser} = \varepsilon_{laser} \times \lambda_n$ (magenta line). All SNR gains are normalized to the corresponding SNR at n=1.

13. References

1 N. P. Isaev, A. R. Melnikov, K. A. Lomanovich, M. V. Dugin, M. Yu. Ivanov, D. N. Polovyanenko, S. L. Veber, M. K. Bowman and E. G. Bagryanskaya, A broadband pulse EPR spectrometer for high-throughput measurements in the X-band, *J. Magn. Reson. Open*, 2023, **14–15**, 100092.

2 G. Jeschke, V. Chechik, P. Ionita, A. Godt, H. Zimmermann, J. Banham, C. R. Timmel, D. Hilger and H. Jung, DeerAnalysis2006 - A comprehensive software package for analyzing pulsed ELDOR data, *Appl. Magn. Reson.*, 2006, **30**, 473–498.

3 S. G. Worswick, J. A. Spencer, G. Jeschke and I. Kuprov, Deep neural network processing of DEER data, *Sci. Adv.*, 2018, **4**, eaat5218.